Acta Mech 227, 2157–2170 (2016)
DOI 10.1007/s00707-016-1627-0

ORIGINAL PAPER

W.-B. Ning · J.-G. Zhang · W.-D. Chen

Dynamics and stability of a functionally graded cylindrical thin shell containing swirling annular fluid flow including initial axial loads

Received: 22 September 2015 / Revised: 17 March 2016 / Published online: 11 April 2016

Abstract Considering initial axial loads, dynamics and stability of an inner functionally graded cylindrical shell conveying swirling fluid (i.e., water) in the annulus between the flexible inner shell and the identical rigid outer shell are investigated by the traveling wave approach. Shell motions are described by Donnell's thin shell equations. The fluid forces associated with shell motions are treated in the frame of the potential flow theory. The theoretical analysis is conducted by the zero-level contour method. The critical velocities of losing stability are determined. The influences of angular flow on the critical axial velocity and axial flow on the critical annular velocity are studied. Moreover, effects of the magnitude and the direction of initial axial loads on the critical velocities are fully discussed.

1 Introduction

Studies on dynamic behavior of coaxial cylindrical shells subjected to annular flow are extensive as a result of such structural elements application in many engineering systems. Tijsseling [1] presented reviews related to the development of fluid–structure interaction in liquid-filled pipe systems. The overview of progress of flow-inducted vibration problems in power plants is provided by Weaver et al. [2]. Dynamics and stability of coaxial cylindrical shells conveying inviscid or viscous fluid were studied with the aid of Fourier transform techniques [3–5]. It is found that annular flow renders the system instability at lower velocities than flow in the inner shell. It is also found that steady viscous forces destabilize the system for annular flow and stabilize it for internal flow dramatically. The effects of system parameters on stability were also discussed. Considering unsteady viscous forces, Chebair et al. [6,7] preformed further studies on the same problem theoretically and experimentally. Further work on the dynamic response of shells conveying fluid was extended to take into account nonlinearity [8–10]. Based on the semi-membrane theory, an approximate theory of annular flow-induced instability of coaxial cylindrical shells was presented [11,12]. Srinivasan [13] firstly studied the aeroelastic stability of a thin cylindrical shell under external helical air flow based on the classical shell theory and linear potential flow theory by travelling wave solutions. This study showed that the system loses stability by coupled-mode flutter. And results obtained were compared with the experimental data [14]. The dynamic behaviors of coaxial cylindrical shells subjected to axial flow were investigated by Bochkarev and Matveenko [15–17], in which the effects of steady viscous forces, annular gaps and physico-mechanical properties of shells

W.-B. Ning (✉) · J.-G. Zhang
School of Mechanical Engineering, Shanghai Jiao Tong University, Shanghai 200240, People's Republic of China
E-mail: wbning@sjtu.edu.cn
Tel.:+8613524719143
Fax:+862134205499

W.-D. Chen
School of Mechanical and Electronic Engineering, Shandong Transport Vocational College,
Weifang 261206, People's Republic of China

on the stability of shells were examined. Moreover, the effects of angular flow on the stability behaviors of coaxial cylindrical shells were studied [18,19]. It is found that the combined action of both velocity components tends to destabilize the system. Considering the circumferential tension caused by rotating shells, Bochkarev and Matveenko [20–23] performed further studies on the same problem. They found that rotation of the shell generally exerts a stabilizing effect in the case of the single shell, but simultaneous rotation of coaxial shells and fluids inside them do not affect the loss of stability. Also, the effect of the elasticity of the outer shells on the character of dynamic behavior of the system was examined. Dynamic stability of isotropic or composite material cylindrical shell carrying a swirling fluid was given by Chen and Bert [24]. The principal finding of their work was that fluid rotation severely decreases stability of the shell–fluid systems.

Functionally graded materials (FGM) have become popular [25] because of advantages of withstanding high-temperature gradient changes and high strength, toughness. Based on the three-dimensional elasticity, Chen et al. [26] developed the laminate approximate mode to investigate the frequency response of a fluid-filled functionally graded shell. Iqbal et al. [27] studied the vibration frequency of the FGM circular shell by using the wave propagation approach. It is found that the frequency of the fluid-filled FGM circular shell is lower than that of the empty FGM circular shell. Furthermore, the influence of the elastic foundation on the frequency was studied [28]. Silva et al. [29] investigated the nonlinear vibration of a fluid-filled FGM circular shell taking into account a time-dependent lateral load and static preload. They found that the internal fluid and compressive stress increase the softening effect of the shell.

Based on the first-order shear deformation theory, the dynamic response of a functionally graded shell subjected to axial flow under thermo-mechanical loads was given [30,31]. The effects of loads, fluid velocity on dynamic characteristics were determined. Shen et al. [32,33] studied the dynamic stability of periodic shells based on the beam mode. It was found that a periodic shell structure enhances its stability.

There are studies of stability and dynamic behavior of isotropic material cylindrical shells subjected to annular flow with only axial velocity component in the literature. However, the influence of a combined action of the axial and the angular velocities of annular flow on stability and dynamic behavior of functionally graded thin cylindrical shells under initial axial loads has not been clearly understood. The effects of initial axial loads on the character of the dynamic behavior of such system and instability flow velocities are also unexplored. In the present study, dynamic behavior of an inner FGM cylindrical shell carrying helical flow with the axial and circumferential velocity components in the annulus between the two shells are studied in a traveling wave solution form. Calculations are conducted by the zero-level contour method. The lowest flow velocities of losing stability (referred to the critical flow velocity) are obtained, and relations of them are examined. These studies will provide useful information for the engineering designs of nuclear reactors, space shuttle, heat exchangers, and others.

2 Problem formulation

Figure 1 shows a schematic diagram of two coaxial FGM cylindrical shells of the same length L. The inner shell with thickness h_i and mean radius of r_i is simply supported at both edges $x = 0$ and $x = L$. The outer circular cylindrical shell with thickness h_o and mean radius r_o is located concentrically as a perfectly rigid shell. The two coaxial shells with the same functionally graded materials are located in an orthogonal coordinate system (O; r, θ, x), in which the origin O is located on the left end at the middle point of the inner shell. x, θ and r are in the axial, circumferential, and radial directions, respectively. The fluid in the annular space between the two shells is considered to be incompressible with the density ρ_f, flowing in x-, θ-directions with velocity components U_o, Ω_o.

2.1 Functionally graded cylindrical shells

The FGM shells are composed of ceramic and metal. The volume fractions of all constitutent materials are related by

$$V_\mathrm{s} + V_\mathrm{c} = 1, \quad V_\mathrm{c} = V_\mathrm{c}(z) = \left(\frac{2z + h}{2h}\right)^N \tag{1}$$

where s, c denote the metal (inner surface) and ceramic (outer surface) constituents; N is the power-law exponent characterizing the metal variation through the shell thickness; z presents a displacement variable of the radius direction. From Eq. (1), the effective elastic modulus E and the mass density ρ can be written as

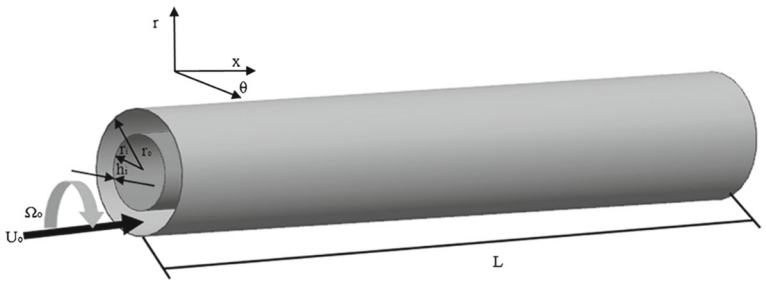

Fig. 1 Schematic diagram of the coaxial FGM cylindrical shells under consideration

$$E(z) = E_s V_s + E_c V_c = E_s + (E_c - E_s)\left(\frac{2z+h}{2h}\right)^N, \tag{2.1}$$

$$\rho(z) = \rho_s V_s + \rho_c V_c = \rho_s + (\rho_c - \rho_s)\left(\frac{2z+h}{2h}\right)^N. \tag{2.2}$$

Poisson' ratio υ is assumed to be constant.

2.2 The governing equations

Based on the classic Donnell's shell theory, the strain components can be represented by [34]

$$\varepsilon_x = u_x + zk_x = \frac{\partial u}{\partial x} + zk_x, \tag{3.1}$$

$$\varepsilon_\theta = u_s + zk_\theta = \frac{\partial v}{r\partial\theta} + \frac{w}{r} + zk_\theta, \tag{3.2}$$

$$\varepsilon_{x\theta} = u_{x\theta} + 2zk_{x\theta} = \frac{\partial u}{r\partial\theta} + \frac{\partial v}{\partial x} + 2zk_{x\theta} \tag{3.3}$$

$$k_x = -\frac{\partial^2 w}{\partial x^2}, \tag{4.1}$$

$$k_\theta = -\frac{\partial^2 w}{r^2\partial\theta^2}, \tag{4.2}$$

$$k_{x\theta} = -\frac{\partial^2 w}{r\partial x\partial\theta} \tag{4.3}$$

where u, v and w are the displacements of the middle surface point of a shell along x, θ, and r direction, respectively, and k_x, k_θ and $k_{x\theta}$ are curvatures and twist of a shell. The forces resultants and bending moments of an FGM cylindrical shell are expressed as

$$\begin{bmatrix} N_x \\ N_\theta \\ N_{x\theta} \\ M_x \\ M_\theta \\ M_{x\theta} \end{bmatrix} = \begin{bmatrix} K_{11} & K_{12} & 0 & K_{14} & K_{15} & 0 \\ K_{21} & K_{22} & 0 & K_{24} & K_{25} & 0 \\ 0 & 0 & K_{33} & 0 & 0 & K_{36} \\ K_{41} & K_{42} & 0 & K_{44} & K_{45} & 0 \\ K_{51} & K_{52} & 0 & K_{54} & K_{55} & 0 \\ 0 & 0 & K_{63} & 0 & 0 & K_{66} \end{bmatrix} [u_x \quad u_s \quad u_{x\theta} \quad k_x \quad k_\theta \quad 2k_{x\theta}] \tag{5}$$

where the stiffness matrix K_{ij} is given by

$$\begin{aligned} K_{11} &= \frac{E_1}{1-\upsilon^2} = K_{22}, \quad K_{12} = \frac{\upsilon E_1}{1-\upsilon^2} = K_{21}, \quad K_{14} = \frac{E_2}{1-\upsilon^2} = K_{25} = K_{41} = K_{52}, \quad K_{15} = \frac{\upsilon E_2}{1-\upsilon^2} \\ &= K_{24} = K_{42} = K_{51}, \\ K_{33} &= \frac{E_1}{2(1+\upsilon)}, \quad K_{36} = \frac{E_2}{2(1+\upsilon)}, \quad K_{44} = \frac{E_3}{1-\upsilon^2} = K_{55}, \quad K_{45} = \frac{\upsilon E_3}{1-\upsilon^2} = K_{54}, \quad K_{63} \\ &= \frac{E_2}{2(1+\upsilon)}, \quad K_{66} = \frac{E_3}{2(1+\upsilon)} \end{aligned} \tag{6}$$

in which

$$E_1 = \int_{-h/2}^{h/2} E(z)\mathrm{d}z = E_m h + \frac{E_\mathrm{c} - E_m}{N+1}h, \quad E_2 = \int_{-h/2}^{h/2} zE(z)\mathrm{d}z = \frac{N(E_\mathrm{c} - E_m)}{2(N+1)(N+2)}h^2,$$
$$E_3 = \int_{-h/2}^{h/2} z^2 E(z)\mathrm{d}z = \frac{E_m h^3}{12} + (E_\mathrm{c} - E_m)h^3\left[\frac{1}{4(N+1)} - \frac{1}{(N+2)} + \frac{1}{(N+3)}\right]. \tag{7}$$

Considering initial axial loads, the motion equations of an FGM cylindrical shell conveying ideal fluid are written as

$$\frac{\partial N_x}{\partial x} + \frac{1}{R}\frac{\partial N_{x\theta}}{\partial \theta} + P\frac{\partial^2 u}{\partial x^2} = \rho_\mathrm{s}\frac{\partial^2 u}{\partial t^2}, \tag{8.1}$$
$$\frac{\partial N_{x\theta}}{\partial x} + \frac{1}{R}\frac{\partial N_\theta}{\partial \theta} + P\frac{\partial^2 v}{\partial x^2} = \rho_\mathrm{s}\frac{\partial^2 v}{\partial t^2}, \tag{8.2}$$
$$\frac{\partial^2 M_x}{\partial x^2} + 2\frac{\partial^2 M_{x\theta}}{R\partial x\partial\theta} + \frac{\partial^2 M_{x\theta}}{R^2\partial\theta^2} - \frac{N_\theta}{R} + P\frac{\partial^2 w}{\partial x^2} = \rho_\mathrm{s}\frac{\partial^2 w}{\partial t^2} + p \tag{8.3}$$

where $\rho_\mathrm{s} = \int_{-h/2}^{h/2}\rho(z)\mathrm{d}z = \rho_\mathrm{s}h + \frac{\rho_\mathrm{c}-\rho_\mathrm{s}}{N+1}h$. t is time. P represents the axial load. p is the perturbation pressure acting on the shells which will be formulated in Sect. 2.3.

Substituting Eq. (5) into Eq. (8.1), the motion equations of an inner shell can be rewritten in one linear matrix operator,

$$\zeta\begin{bmatrix} u_\mathrm{i/o} \\ v_\mathrm{i/o} \\ w_\mathrm{i/o} \end{bmatrix} = \begin{bmatrix} 0 \\ 0 \\ p \end{bmatrix}, \tag{9}$$

where

$$\zeta = \begin{bmatrix} \zeta_{11} & \zeta_{12} & \zeta_{13} \\ \zeta_{21} & \zeta_{22} & \zeta_{23} \\ \zeta_{31} & \zeta_{32} & \zeta_{33} \end{bmatrix} \tag{10}$$

in which $\Delta = \frac{\partial^2}{\partial x^2} + \frac{1}{r^2}\frac{\partial^2}{\partial\theta^2}$,

$$\zeta_{11} = \frac{E_1}{1-\upsilon^2}\left[(1+P)\frac{\partial^2}{\partial x^2} + \frac{1-\upsilon}{2r^2}\frac{\partial^2}{\partial\theta^2} - \rho_\mathrm{s}\frac{1-\upsilon^2}{E_1}\frac{\partial^2}{\partial t^2}\right], \quad \zeta_{12} = \frac{E_1}{1-\upsilon^2}\left[\frac{1+\upsilon}{2r}\frac{\partial^2}{\partial x\partial\theta}\right],$$
$$\zeta_{13} = \frac{E_1}{1-\upsilon^2}\left[\frac{\upsilon}{r}\frac{\partial}{\partial x} - \frac{E_2}{E_1}\frac{\partial^3}{\partial x^3} - \frac{E_2}{r^2E_1}\frac{\partial^3}{\partial x\partial\theta^2}\right], \quad \zeta_{21} = \frac{E_1}{1-\upsilon^2}\left[\frac{1+\upsilon}{2r}\frac{\partial^2}{\partial x\partial\theta}\right],$$
$$\zeta_{22} = \frac{E_1}{1-\upsilon^2}\left[(1+P)\frac{1-\upsilon}{2}\frac{\partial^2}{\partial x^2} + \frac{1}{r^2}\frac{\partial^2}{\partial\theta^2} - \rho_\mathrm{s}\frac{1-\upsilon^2}{E_1}\frac{\partial^2}{\partial t^2}\right],$$
$$\zeta_{23} = \frac{E_1}{1-\upsilon^2}\left[\frac{1}{r^2}\frac{\partial}{\partial\theta} - \frac{E_2}{rE_1}\frac{\partial^3}{\partial x^2\partial\theta} - \frac{E_2}{r^3E_1}\frac{\partial^3}{\partial\theta^3}\right],$$
$$\zeta_{31} = \frac{E_1}{1-\upsilon^2}\left[\frac{\upsilon}{r}\frac{\partial}{\partial x} - \frac{E_2}{E_1}\left(\frac{\partial^3}{\partial x^3} + \frac{1}{r^2}\frac{\partial^3}{\partial x\partial\theta^2}\right)\right], \quad \zeta_{32} = \frac{E_1}{1-\upsilon^2}\left[\frac{1}{r^2}\frac{\partial}{\partial\theta} - \frac{E_2}{rE_1}\left(\frac{\partial^3}{\partial x^2\partial\theta} + \frac{1}{r^2}\frac{\partial^3}{\partial\theta^3}\right)\right],$$
$$\zeta_{33} = \frac{E_1}{1-\upsilon^2}\left[-P\frac{\partial^2}{\partial x^2} + \frac{E_3}{E_1}\Delta\Delta + \rho_\mathrm{s}\frac{1-\upsilon^2}{E_1}\frac{\partial^2}{\partial t^2} + \frac{1}{r^2} - \frac{2\upsilon E_2}{rE_1}\frac{\partial^2}{\partial x^2} - \frac{2E_2}{r^3E_1}\frac{\partial^2}{\partial\theta^2}\right].$$

2.3 Perturbation pressure

Note that the fluid is inviscid and incompressible and the flow is assumed to be a potential flow. The potential Ψ consists of two components: the steady state potential of the fluid which is characterized by the axial constant velocity U_o and tangential constant velocity $V_\mathrm{o} = \Omega_\mathrm{o} \times r$ and unsteady component Φ associated with shell motions. Thus,

$$\Psi = U_\mathrm{o}x + V_\mathrm{o}\theta + \Phi. \tag{11}$$

A perturbation potential Φ satisfies the Laplace equation $\nabla^2\Phi = 0.\nabla^2$ denotes the Laplace operator. The solution of the Laplace equation is given in the form of the traveling wave $\Phi = \Phi(r)\exp[-i(\lambda x + n\theta - \omega t)]$. Here, $i = (-1)^{1/2}.\lambda$, n, and ω are the axial wavenumber, circumferential wavenumber, and frequency.

Substituting the traveling wave solution into the Laplace equation, one can arrive at

$$\Phi(r) = AI_n(\lambda r) + BK_n(\lambda r) \tag{12}$$

where I_n and K_n are the modified Bessel functions of the first and second kind and order n. A, B are constants which will be determined subsequently.

It is noted that though the present paper is concerned with dynamic stability of the inner cylindrical shell, the analysis to be presented here involves the inner shell and outer shell in order to utilize nonpenetration conditions of the two shells' interaction with fluid.

Based on the condition of impermeability on the fluid–shell interfaces, the radial velocity of the flow must be equal to the radial velocity of the shell wall,

$$V_{ri} = \partial\Phi/\partial r = Dw_\mathrm{i}/Dt = \frac{\partial w_\mathrm{i}}{\partial t} + \frac{V_\mathrm{o}}{r}\frac{\partial w_\mathrm{i}}{\partial\theta} + U_\mathrm{o}\frac{\partial w_\mathrm{i}}{\partial x}\ (r = r_\mathrm{i}), \tag{13.1}$$

$$V_{ro} = \partial\Phi/\partial r = Dw_\mathrm{o}/Dt = \frac{\partial w_\mathrm{o}}{\partial t} + \frac{V_\mathrm{o}}{r}\frac{\partial w_\mathrm{o}}{\partial\theta} + U_\mathrm{o}\frac{\partial w_\mathrm{o}}{\partial x}\ (r = r_\mathrm{o}) \tag{13.2}$$

where the subscripts i and o indicate the inner shell and the outer shell, respectively.

Allowing for Eq. (12), introducing the traveling wave solution Φ in Eqs. (13.1, 13.2), the flowing equations are obtained

$$A_1 I_n'(\lambda r_\mathrm{i}) + B_1 K_n'(\lambda r_\mathrm{i}) = \frac{\partial w_\mathrm{i}}{\partial t} + \frac{V_\mathrm{o}}{r}\frac{\partial w_\mathrm{i}}{\partial\theta} + U_\mathrm{o}\frac{\partial w_\mathrm{i}}{\partial x}, \tag{14.1}$$

$$A_1 I_n'(\lambda r_\mathrm{o}) + B_1 K_n'(\lambda r_\mathrm{o}) = \frac{\partial w_\mathrm{o}}{\partial t} + \frac{V_\mathrm{o}}{r}\frac{\partial w_\mathrm{o}}{\partial\theta} + U_\mathrm{o}\frac{\partial w_\mathrm{o}}{\partial x} \tag{14.2}$$

where the prime denotes the differentiation with respect to the argument of the primed function;

$$A_1 = \frac{1}{\Gamma}\left[K_n'(\lambda r_\mathrm{o})\left(\frac{\partial w_\mathrm{i}}{\partial t} + \frac{V_\mathrm{o}}{r}\frac{\partial w_\mathrm{i}}{\partial\theta} + U_\mathrm{o}\frac{\partial w_\mathrm{i}}{\partial x}\right) - K_n'(\lambda r_\mathrm{i})\left(\frac{\partial w_\mathrm{o}}{\partial t} + \frac{V_\mathrm{o}}{r}\frac{\partial w_\mathrm{o}}{\partial\theta} + U_\mathrm{o}\frac{\partial w_\mathrm{o}}{\partial x}\right)\right], \tag{15.1}$$

$$B_1 = \frac{1}{\Gamma}\left[I_n'(\lambda r_\mathrm{i})\left(\left(\frac{\partial w_\mathrm{o}}{\partial t} + \frac{V_\mathrm{o}}{r}\frac{\partial w_\mathrm{o}}{\partial\theta} + U_\mathrm{o}\frac{\partial w_\mathrm{o}}{\partial x}\right)\right) - I_n'(\lambda r_\mathrm{o})\left(\frac{\partial w_\mathrm{i}}{\partial t} + \frac{V_\mathrm{o}}{r}\frac{\partial w_\mathrm{i}}{\partial\theta} + U_\mathrm{o}\frac{\partial w_\mathrm{i}}{\partial x}\right)\right], \tag{15.2}$$

$$\Gamma = I_n'(\lambda r_\mathrm{i})K_n'(\lambda r_\mathrm{o}) - I_n'(\lambda r_\mathrm{o})K_n'(\lambda r_\mathrm{i}). \tag{15.3}$$

After certain manipulations, the potential Φ can be rewritten as

$$\Phi = \frac{1}{\Gamma}\Gamma_1\left(\frac{\partial w_\mathrm{i}}{\partial t} + \frac{V_\mathrm{o}}{r}\frac{\partial w_\mathrm{i}}{\partial\theta} + U_\mathrm{o}\frac{\partial w_\mathrm{i}}{\partial x}\right) + \frac{1}{\Gamma}\Gamma_2\left(\frac{\partial w_\mathrm{o}}{\partial t} + \frac{V_\mathrm{o}}{r}\frac{\partial w_\mathrm{o}}{\partial\theta} + U_\mathrm{o}\frac{\partial w_\mathrm{o}}{\partial x}\right) \tag{16}$$

where $\Gamma_1 = I_n(\lambda r)K_n'(\lambda r_\mathrm{o}) - I_n'(\lambda r_\mathrm{o})K_n(\lambda r)$, $\Gamma_2 = I_n'(\lambda r_\mathrm{i})K_n(\lambda r) - I_n(\lambda r)K_n'(\lambda r_\mathrm{i})$.

Based on Eq. (8.1), the velocity components of the flow field are given by

$$V_x = U_\mathrm{o} + \frac{\partial\Phi}{\partial x}, \quad V_\theta = V_\mathrm{o} + \frac{\partial\Phi}{r\partial\theta}, V_r = \frac{\partial\Phi}{\partial r}. \tag{17}$$

The perturbation pressure is determined from the Bernoulli equation,

$$\frac{\partial\Phi}{\partial t} + \frac{1}{2}V^2 + \frac{P'}{\rho} = \frac{P_\mathrm{s}}{\rho}, \tag{18}$$

where $V = V_x^2 + V_\theta^2 + V_r^2$. P_s is the stagnation pressure. $P' = \overline{P} + p$. $\overline{P}$ and p are the mean pressure and the perturbation pressure, respectively.

Substituting the quantities V, P' into Eq. (18) and neglecting second-order terms—by considering motions of the shell to be small—Eq. (18) yields

$$P_{\mathrm{s}} = \overline{p} + \frac{1}{2}\rho\left(U_{\mathrm{o}}^2 + V_{\mathrm{o}}^2\right), \tag{19.1}$$

$$p = -\rho_{\mathrm{f}}\left(\frac{\partial}{\partial t} + \frac{V_{\mathrm{o}}}{r}\frac{\partial}{\partial \theta} + U_{\mathrm{o}}\frac{\partial}{\partial x}\right)\Phi. \tag{19.2}$$

Introducing Eq. (16) in Eq. (19.2), the perturbation pressure on the inner shell or outer shell is given by

$$\begin{aligned} p_{\mathrm{i}} = &-\frac{\rho_{\mathrm{f}}}{\Gamma}\left(\frac{\partial}{\partial t} + \frac{V_{\mathrm{o}}}{r}\frac{\partial}{\partial \theta} + U_{\mathrm{o}}\frac{\partial}{\partial x}\right)^2 \left\{\left[I_n(\lambda r_{\mathrm{i}})K_n'(\lambda r_{\mathrm{o}}) - I_n'(\lambda r_{\mathrm{o}})K_n(\lambda r_{\mathrm{i}})\right] w_{\mathrm{i}}\right. \\ &\left. + \left[I_n'(\lambda r_{\mathrm{i}})K_n(\lambda r_{\mathrm{i}}) - I_n(\lambda r_{\mathrm{i}})K_n'(\lambda r_{\mathrm{i}})\right] w_{\mathrm{o}}\right\}, \end{aligned} \tag{20}$$

$$\begin{aligned} p_{\mathrm{o}} = &-\frac{\rho_{\mathrm{f}}}{\Gamma}\left(\frac{\partial}{\partial t} + \frac{V_{\mathrm{o}}}{r}\frac{\partial}{\partial \theta} + U_{\mathrm{o}}\frac{\partial}{\partial x}\right)^2 \left\{\left[I_n(\lambda r_{\mathrm{o}})K_n'(\lambda r_{\mathrm{o}}) - I_n'(\lambda r_{\mathrm{o}})K_n(\lambda r_{\mathrm{o}})\right] w_{\mathrm{i}}\right. \\ &\left. + \left[I_n'(\lambda r_{\mathrm{i}})K_n(\lambda r_{\mathrm{o}}) - I_n(\lambda r_{\mathrm{o}})K_n'(\lambda r_{\mathrm{i}})\right] w_{\mathrm{o}}\right\}. \end{aligned} \tag{21}$$

When one of the two coaxial shells is perfectly rigid, the expression (21) can be simplified.

(i) elastic inner and perfectly rigid outer shells. In this case, the condition w_{o} is zero. The perturbation pressure on the inner shell is rewritten as

$$p_{\mathrm{i}} = -\frac{\rho_{\mathrm{f}}}{\Gamma}\left(\frac{\partial}{\partial t} + \frac{V_{\mathrm{o}}}{r}\frac{\partial}{\partial \theta} + U_{\mathrm{o}}\frac{\partial}{\partial x}\right)^2 \left[I_n(\lambda r_{\mathrm{i}})K_n'(\lambda r_{\mathrm{o}}) - I_n'(\lambda r_{\mathrm{o}})K_n(\lambda r_{\mathrm{i}})\right] w_{\mathrm{i}}. \tag{22.1}$$

(ii) elastic outer and perfectly rigid inner shells. Here, the condition w_{i} equals zero. The perturbation pressure on the outer shell is rewritten as

$$p_{\mathrm{o}} = -\frac{\rho_{\mathrm{f}}}{\Gamma}\left(\frac{\partial}{\partial t} + \frac{V_{\mathrm{o}}}{r}\frac{\partial}{\partial \theta} + U_{\mathrm{o}}\frac{\partial}{\partial x}\right)^2 \left[I_n'(\lambda r_{\mathrm{i}})K_n(\lambda r_{\mathrm{o}}) - I_n(\lambda r_{\mathrm{o}})K_n'(\lambda r_{\mathrm{i}})\right] w_{\mathrm{o}}. \tag{22.2}$$

2.4 Dynamics and stability analysis

An inner shell with simply supported boundary conditions is considered; the boundary conditions at two edges $x = 0, L$ are:

$$v = w = N_x = M_x = 0. \tag{23}$$

Displacement components u, v, and w of the inner shell fulfilling approximately simply supported boundary conditions can be expanded in the form of the traveling wave [35],

$$\begin{bmatrix} u_{\mathrm{i/o}} \\ v_{\mathrm{i/o}} \\ w_{\mathrm{i/o}} \end{bmatrix} = \begin{bmatrix} u_{mn}\exp[-i(\lambda x + n\theta - \omega t)] \\ v_{mn}\exp[-i(\lambda x + n\theta - \omega t)] \\ w_{mn}\exp\left[-i\left(\lambda x + n\theta - \omega t + \pi/2\right)\right] \end{bmatrix} \left(\lambda = \frac{m\pi}{L}\right). \tag{24}$$

In order to make the dimensionless analysis, the follow dimensionless quantities are defined:

$$\begin{aligned} &\tau = r_{\mathrm{i}}\sqrt{\frac{\rho_{\mathrm{s}}(1-\upsilon^2)}{E_1}}, \quad \overline{t} = \frac{t}{\tau}, \overline{h} = \frac{h}{r_{\mathrm{i}}}, \quad \overline{x} = \frac{x}{r_{\mathrm{i}}}, \quad \overline{L} = \frac{L}{r_{\mathrm{i}}}, \quad \overline{r} = \frac{r}{r_{\mathrm{i}}}, \quad \overline{p} = \frac{\tau^2}{\rho_{\mathrm{s}} r_{\mathrm{i}}^2}p, \\ &\overline{U_{\mathrm{o}}} = \frac{U_{\mathrm{o}}\tau}{r_{\mathrm{i}}}, \quad \overline{V_{\mathrm{o}}} = \frac{V_{\mathrm{o}}\tau}{r_{\mathrm{i}}}, \quad k = \frac{r_{\mathrm{o}} - r_{\mathrm{i}}}{r_{\mathrm{i}}}, \quad \overline{\omega} = \omega\tau, \\ &\begin{bmatrix} \overline{u_{\mathrm{i/o}}} \\ \overline{v_{\mathrm{i/o}}} \\ \overline{w_{\mathrm{i/o}}} \end{bmatrix} = \frac{1}{r_{\mathrm{i}}}\begin{bmatrix} u_{\mathrm{i/o}} \\ v_{\mathrm{i/o}} \\ w_{\mathrm{i/o}} \end{bmatrix}. \end{aligned} \tag{25}$$

Note that the outer shell is perfectly rigid, allowing for Eqs. (22.1), (24), (25), and (9) is reformulated in the dimensionless form

$$\zeta \begin{bmatrix} \overline{u_{\mathrm{i}}} \\ \overline{v_{\mathrm{i}}} \\ -i\overline{w_{\mathrm{i}}} \end{bmatrix} = \begin{bmatrix} 0 \\ 0 \\ 0 \end{bmatrix} \tag{26}$$

where the entries $\zeta_{i,j}$ in the operator matrix ζ are given by

$$\begin{aligned}
&\zeta_{11} = -\left[1 + \frac{1-\upsilon^2}{\overline{E_1}}P\right]\lambda^2 - \frac{1-\upsilon}{2}n^2 + \overline{\omega}^2, \quad \zeta_{12} = -\frac{1+\upsilon}{2}\lambda n, \quad \zeta_{13} = -i\upsilon\lambda - \frac{\overline{E_2}}{\overline{E_1}}i\lambda^3 - \frac{\overline{E_2}}{\overline{E_1}}i\lambda n^2, \\
&\zeta_{21} = -\frac{1+\upsilon}{2}\lambda n, \quad \zeta_{22} = -\left[\frac{1-\upsilon}{2} + \frac{1-\upsilon^2}{\overline{E_1}}P\right]\lambda^2 - n^2 + \overline{\omega}^2, \quad \zeta_{23} = -in - \frac{\overline{E_2}}{\overline{E_1}}i\lambda^2 n - \frac{\overline{E_2}}{\overline{E_1}}in^3, \\
&\zeta_{31} = -i\upsilon\lambda - \frac{\overline{E_2}}{\overline{E_1}}i\lambda^3 - \frac{\overline{E_2}}{\overline{E_1}}i\lambda n^2, \\
&\zeta_{32} = -in - \frac{\overline{E_2}}{\overline{E_1}}i\lambda^2 n - \frac{\overline{E_2}}{\overline{E_1}}in^3, \quad \zeta_{33} = \frac{1-\upsilon^2}{\overline{E_1}}P\lambda^2 + 1 + \frac{\overline{E_3}}{\overline{E_1}}\left(\lambda^2 + n^2\right)^2 - \overline{\omega}^2 + 2\frac{\overline{E_2}}{\overline{E_1}}\upsilon\lambda^2 \\
&\qquad +2\frac{\overline{E_2}}{\overline{E_1}}n^2 + \frac{\overline{\Gamma}_1}{\overline{\Gamma}}\frac{1}{\overline{h}}\frac{\rho_{\mathrm{f}}}{\rho_{\mathrm{s}}}\left(\overline{\omega} - \lambda\overline{U_{\mathrm{o}}} - n\overline{V}_{\mathrm{o}}\right)^2,
\end{aligned} \tag{27}$$

Considering the condition for a nontrivial solution of Eq. (26), the determinant of the operator matrix must be equal to zero.

$$|\zeta| = 0 \tag{28}$$

The left hand side of Eq. (28) is a sixth-order polynomial of variable $\overline{\omega}$. The dispersion relation is evaluated by the zero-level contour method. For a given value of $\overline{V_{\mathrm{o}}}$ (or $\overline{U_0}$), the contour plot of $\overline{\omega}$ versus $\overline{U_0}$ (or $\overline{V_0}$) is realized by the method.

3 Results and discussion

3.1 Validation

Based on the shell mode, few detailed reports on stability and dynamics of swirling fluid-conveying FGM cylindrical shells taking into account initial loads are available in the literature; an exact comparison of the present results with existing results is difficult. In order to obtain a comparison with existing results, FGM cylindrical shells can be simplified to the homogenous shells subjected to annular flow. The relevant geometric and material parameters for the system are as follows:

$$\begin{aligned}
&L = 1\ \mathrm{m}, \quad r_{\mathrm{o}} = 0.1\ \mathrm{m}, \quad h_{\mathrm{i}} = h_{\mathrm{o}} = 5 \times 10^{-4}\ \mathrm{m}, \quad k = r_0 - r_{\mathrm{i}}/r_{\mathrm{i}}, \quad r_{\mathrm{i}} = 9.091 \times 10^{-2}\ \mathrm{m}\ (k = 0.1), \\
&E = 2.0 \times 10^{11}\ P_{\mathrm{a}}, \quad \upsilon = 0.3, \quad \rho_{\mathrm{s}} = 7800\ \mathrm{kgm}^{-3}, \quad \rho_{\mathrm{f}} = 1000\ \mathrm{kgm}^{-3}.
\end{aligned}$$

In this case, the outer shell is perfectly rigid, and the annular flow between the two shells has only an axial velocity component.

Omitting initial loads, the operator matrix ζ in Eq. (26) is rewritten, and the entries are:

$$\begin{aligned}
&\zeta_{11} = -\lambda^2 - \frac{1-\upsilon}{2}n^2 + \overline{\omega}^2, \quad \zeta_{12} = -\frac{1+\upsilon}{2}\lambda n, \quad \zeta_{13} = -i\upsilon\lambda, \\
&\zeta_{21} = -\frac{1+\upsilon}{2}\lambda n, \quad \zeta_{22} = -\frac{1-\upsilon}{2}\lambda^2 - n^2 + \overline{\omega}^2, \quad \zeta_{23} = -in, \\
&\zeta_{31} = -i\upsilon\lambda, \quad \zeta_{32} = -in, \quad \zeta_{33} = 1 + \frac{\overline{h}^2}{12}\left(\lambda^2 + n^2\right)^2 - \overline{\omega}^2 + \frac{\overline{\Gamma}_1}{\overline{\Gamma}}\frac{1}{\overline{h}}\frac{\rho_{\mathrm{f}}}{\rho_{\mathrm{s}}}\left(\overline{\omega} - \lambda\overline{U_{\mathrm{o}}}\right)^2.
\end{aligned} \tag{29}$$

These results obtained for of the simply supported inner shell are listed in Table 1 and are compared with those in the literature. From Table 1, it can be noted that the present results are in reasonable agreement with existing results.

Table 1 Comparison of dimensionless critical axial velocities of shells with simply supported boundary conditions

Gap ratio k	Critical velocity (by divergence)		Critical velocity (by flutter)	
	U_o	U_o [present]	U_o	U_o [present]
0.1	0.0102 [12]	0.0110	0.0540 [12]	0.0570

To verify the present algorithm, the critical angular velocity of an inner shell interacting with an annular flow with a rigid outer shell is calculated. The following geometric and material properties are adopted:

$$L = 2.42\ \text{m},\quad r_o = 0.305\ \text{m},\quad r_i = 0.1\ \text{m},\quad h_i = 5\times 10^{-4}\,\text{m},\quad h_o = 8\times 10^{-4}\,\text{m},\quad k = r_0 - r_i/r_i = 2.05,$$
$$E_i = 7.0\times 10^{10}\ P_a,\quad \upsilon = 0.33,\quad \rho_s = 2750\ \text{kgm}^{-3},\quad \rho_f = 245\ \text{kgm}^{-3}.$$

The angular critical velocity calculated ($1736\,\text{min}^{-1}$) is in good agreement with the velocity value($1800\,\text{min}^{-1}$) in the literature [14].

In order to ascertain the nature frequency obtained, comparisons are carried out for a fluid-filled FGM shell with existing results [27]. In this case, the FGM shell is simply supported with the following geometric properties: $L/R = 20,\ h/R = 0.002$.

The type II FGM shells are composed of nickel at the inner surface and stainless steel at the outer surface. The materials properties adopted are:

$$E_1 = 2.07788\times 10^{11}\ P_a,\quad E_2 = 3.8\times 10^{11}\ P_a,\quad \upsilon_1 = 0.317756,\quad \upsilon_2 = 0.3100,$$
$$\rho_1 = 8166\ \text{kgm}^{-3},\quad \rho_2 = 8900\ \text{kgm}^{-3},\quad \rho_f = 1000\ \text{kgm}^{-3},\quad c = 1500\,\text{ms}^{-1}.$$

In this case, the FGM shell is filled with stagnant fluid (ρ_f). The hydrodynamic pressure p_i^i exerted on the inwall of the FGM shell by the internal fluid can be expressed as

$$p_i^i = -\rho_f \frac{I_n(\lambda)}{I_n'(\lambda)}\frac{\partial^2 w_i}{\partial t^2}. \tag{30}$$

The operation matrix ζ in Eq. (26) is rewritten, and the entries are:

$$\zeta_{11} = -\lambda^2 - \frac{1-\upsilon}{2}n^2 + \overline{\omega}^2,\quad \zeta_{12} = -\frac{1+\upsilon}{2}\lambda n,\quad \zeta_{13} = -i\upsilon\lambda - \frac{\overline{E_2}}{\overline{E_1}}i\lambda^3 - \frac{\overline{E_2}}{\overline{E_1}}i\lambda n^2,$$
$$\zeta_{21} = -\frac{1+\upsilon}{2}\lambda n,\quad \zeta_{22} = -\frac{1-\upsilon}{2}\lambda^2 - n^2 + \overline{\omega}^2,\quad \zeta_{23} = -in - \frac{\overline{E_2}}{\overline{E_1}}i\lambda^2 n - \frac{\overline{E_2}}{\overline{E_1}}in^3,$$
$$\zeta_{31} = -i\upsilon\lambda - \frac{\overline{E_2}}{\overline{E_1}}i\lambda^3 - \frac{\overline{E_2}}{\overline{E_1}}i\lambda n^2,$$
$$\zeta_{32} = -in - \frac{\overline{E_2}}{\overline{E_1}}i\lambda^2 n - \frac{\overline{E_2}}{\overline{E_1}}in^3,\quad \zeta_{33} = 1 + \frac{\overline{E_3}}{\overline{E_1}}\left(\lambda^2 + n^2\right)^2 - \overline{\omega}^2 + 2\frac{\overline{E_2}}{\overline{E_1}}\upsilon\lambda^2 + 2\frac{\overline{E_2}}{\overline{E_1}}n^2$$
$$-\frac{1}{\overline{h}}\frac{\rho_f}{\rho_s}\frac{\mathrm{I}_n(\lambda)}{\mathrm{I}_n'(\lambda)}\overline{\omega}^2, \tag{31}$$

The results calculated are summarized in Table 2, where they are compared with those in the literature. The maximum error is no more than 8 %. As can be seen, reasonable agreement is obtained in the comparisons.

3.2 Dynamics and stability analysis of the inner shell subjected to an annular flow

In this case, the outer shell is considered perfectly rigid; dynamics and stability of the outer shell subjected to annular flow are analyzed without incorporating initial loads effects.

In each subsection below, the materials properties adopted are:

$$E_m = 2\times 10^{11}\ P_a,\quad E_c = 3.8\times 10^{11}\ P_a,\quad \upsilon = \upsilon_m = \upsilon_c = 0.3,\quad \rho_m = 8870\ \text{kgm}^{-3},$$
$$\rho_c = 4000\ \text{kgm}^{-3},\quad \rho_f = 1000\ \text{kgm}^{-3}.$$

Table 2 Comparison of the frequency of the type II FGM shell with the simply supported boundary condition, $N = 1$

m	n	Uncoupled frequency		Coupled frequency	
1	2	4.4795 [27]	4.4731 [present]	0.9061 [27]	0.8786 [present]
1	3	4.1562 [27]	4.3932 [present]	0.9640 [27]	1.0384 [present]
1	4	7.0380 [27]	7.2688 [present]	1.8298 [27]	1.9170 [present]
1	5	11.2407 [27]	11.3425 [present]	3.2087 [27]	3.2750 [present]

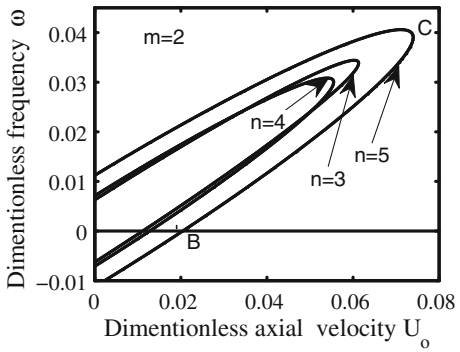

Fig. 2 Variation in the dimensionless frequency with the dimensionless axial velocity for a simply supported shell, $\overline{\Omega_o} = 0$, $N = 1$

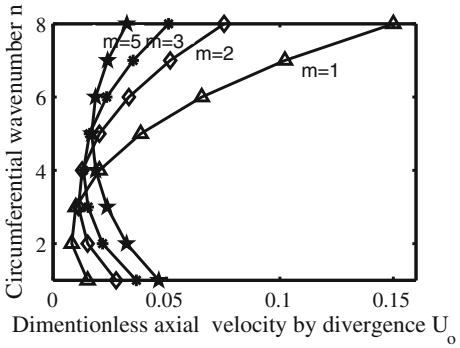

Fig. 3 Circumferential wave number against axial flow velocity (by divergence) at $\overline{\Omega_o} = 0$, $N = 1$

Geometric parameters are given by

$$L = 1\ \text{m},\ r_o = 1 \times 10^{-1}\ \text{m},\ h_i = h_o = 5 \times 10^{-4}\,\text{m},\quad k = r_0 - r_i/r_i, r_i = 9.091 \times 10^{-2}\,\text{m}\ (k = 0.1).$$

In this case, when the fluid flow has only an axial velocity component, the results obtained showing the variation in the dimensionless frequency with the dimensionless axial flow velocity are plotted in Fig. 2 by solving Eq. (28). For the ceramic–metal FGM shell at $n = 5$, it is noted that when the back traveling wave crosses the frequency $\overline{\omega} = 0$ line at the point B, the system loses stability by divergence or buckling. The forward and backward traveling wave frequencies meet at the point C where immediately after point C the frequency becomes a complex conjugate pair, indicating a coupled-mode flutter of the system. Similar results are given for different circumferential wavenumbers n in Fig. 2. It should be noted that the negative imaginary part of the solutions of the Eq. (28) cannot merge when the system loses stability by divergence. The judgment criterion of the instability by divergence is different from that in the literature [3]. In order to determine the critical flow velocity associated with the mode, the flow velocities with different modes (m, n) are shown in Figs. 3 and 4. It is found that when the mode (m, n) is $(1, 2)$, the critical velocity by divergence is $\overline{U_o} = 0.0082$. And the critical velocity by flutter is $\overline{U_o} = 0.0555$ associated with the mode (2, 4). It is also found that the value of the axial wavenumber m associated with the critical velocity of an FGM shell is different from the corresponding value of an isotropic material shell (usually $m = 1$) [12].

In the case when the fluid flow has only an angular velocity component, Figs. 5 and 6 illustrate similar results of the dimensionless frequency against the dimensionless angular flow velocity. It can be seen that the

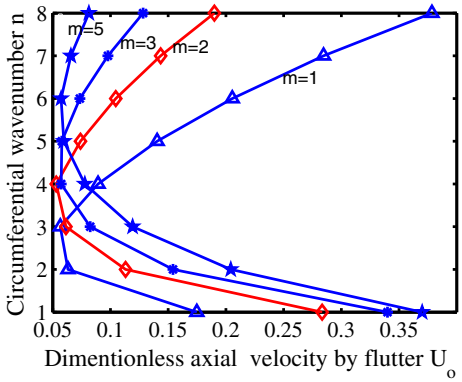

Fig. 4 Circumferential wave number against axial flow velocity (by flutter) at $\overline{\Omega_o} = 0,\ N = 1$

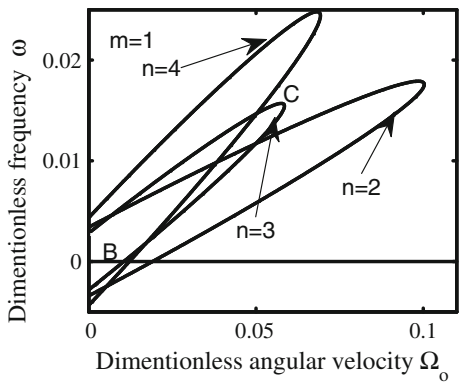

Fig. 5 Variation in the dimensionless frequency with the dimensionless angular velocity for a simply supported shell, $\overline{U_o} = 0,\ N = 1$

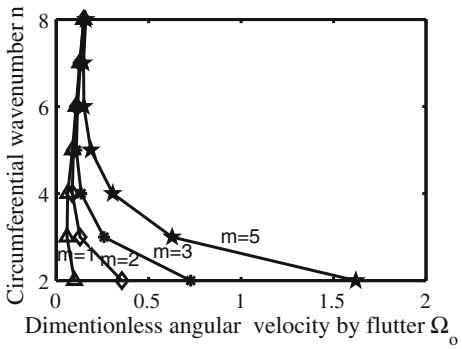

Fig. 6 Circumferential wave number against angular flow velocity (by flutter) at $\overline{U_o} = 0,\ N = 1$

loss of stability of the system occurs first by divergence and then by flutter at the critical angular velocity $\overline{\Omega_o} = 0.0584$ associated with the mode (1, 3).

In order to investigate the effect of fluid rotation on the critical axial velocity, the variation curves of the frequency against the axial flow velocity are plotted in Fig. 7. It is seen that with the appearance of angular rotation flow the frequencies of the forward and backward waves are different in magnitude at $\overline{U_o} = 0$, and the critical axial velocity decreases rapidly. It is also seen that when the angular flow velocity reaches a certain value the system loses stability by flutter only. At the same time, with the appearance of axial velocity, the critical angular velocity of losing stability reduced correspondingly. Figure 8 shows the correlations between the critical axial velocity and angular velocity of losing stability. As can be observed, the stability boundary line is established by assigning that one of the two velocity components is a fixed value and then searching for the critical value of the other velocity.

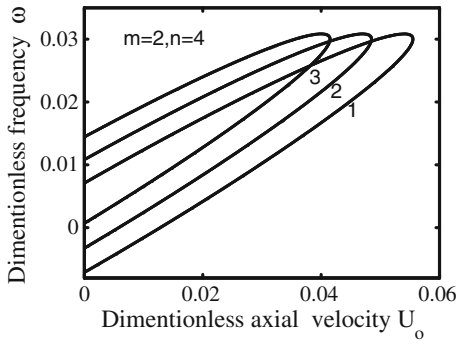

Fig. 7 Variation in the dimensionless frequency with the dimensionless axial velocity for a simply supported shell, $N = 1, 1 : \overline{\Omega_o} = 0, 2 : \overline{\Omega_o} = 0.0113 : \overline{\Omega_o} = 0.022$

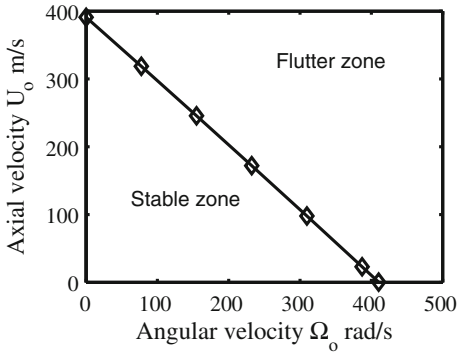

Fig. 8 Correlation curves of the critical axial velocity versus the critical angular velocity for a simply supported shell, $N = 1$

Table 3 Effect of power-law index N on the critical velocities

Critical flow velocities	$N = 0.5$	$N = 1$	$N = 2$	$N = 3$	$N = 4$
U_o ($\Omega_o = 0$ by divergence)	60.57 (m/s)	57.71 (m/s)	54.75 (m/s)	53.23 (m/s)	51.52 (m/s)
U_o ($\Omega_o = 0$ by flutter)	436.52 (m/s)	390.57 (m/s)	354.14 (m/s)	338.09 (m/s)	328.96 (m/s)
Ω_o ($U_o = 0$ by flutter)	461.03 (rad/s)	410.27 (rad/s)	373.67 (rad/s)	356.89 (rad/s)	322.14 (rad/s)
U_o ($\overline{\Omega_o} = 0.0022$ by flutter)	273.61 (m/s)	245.60 (m/s)	224.79 (m/s)	215.90 (m/s)	211.47 (m/s)

With the same physical and geometric data, the effect of different values of power-law index N on the critical flow velocity is summarized in Table 3. From Table 3, it can be seen that the critical flow velocities decrease with the increase of N. This property reflects the real property of the ceramic–metal FGM shell, because the higher value of N corresponds to a metal-richer shell which usually has less stiffness than a ceramic-richer shell.

3.3 Effects of initial axial loads

In this calculation, the axial load is expressed as

$$P = T P_{\text{cr}} \tag{32}$$

where $P_{\text{cr}} = \frac{E_m h^2}{r_i \sqrt{3(1-\upsilon^2)}}$ indicates the static axial buckling load of the cylindrical shell [36] and T defines the axial loading factor. The sign of the axial loading factor T is ('−'), indicating the compressive load, but the sign of the axial loading factor T is ('+'), indicating the tensile load.

Figures 9 and 10 show the effects of the axial compressive load on the critical flow velocities. From the two figures, it is observed that the axial compressive load decreases the critical flow velocities, i.e., the system becomes more unstable. The critical axial compressive factor T is determined as shown in Fig. 11. It

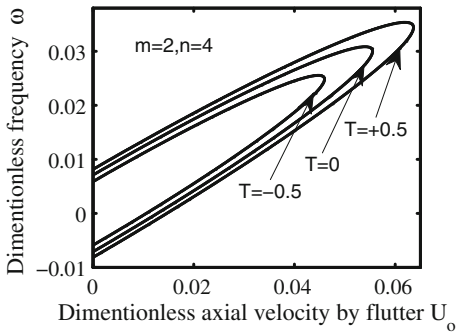

Fig. 9 Variation in the dimensionless frequency with the dimensionless axial velocity for a simply supported shell under different axial compressive load factors, $N = 1$

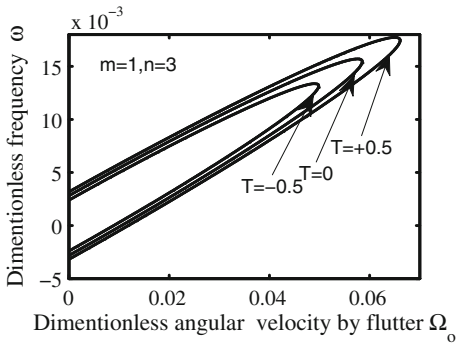

Fig. 10 Variation in the dimensionless frequency with the dimensionless angular velocity for a simply supported shell under different axial compressive load factors, $N = 1$

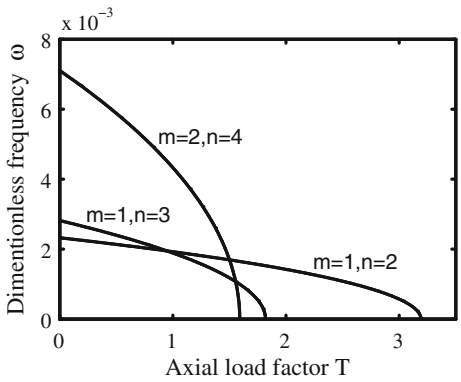

Fig. 11 Variation in the dimensionless frequency with the axial compressive load factor at $\overline{U_o} = 0, \overline{\Omega_o} = 0,\ N = 1$

is observed that by increasing the value of T ('−') gradually the frequency becomes smaller till zero where the corresponding axial compressive factor is the critical axial compressive factor. It is found that the axial compressive factors for the different critical flow velocities are different in general.

Figure 12 shows the effects of a combined action of the axial flow and the angular rotation of flow on the stability behavior of the system under initial axial loads. As can be seen, the variation tendency of the curves under the different directions of axial loads is different. It is seen that the critical axial velocity decreases rapidly with the increase in critical angular velocity. It is also seen that the overall velocity instability of the system including the axial and angular velocity components reduces markedly as the direction of the axial load changes from tensile ('+') to compressive ('−').

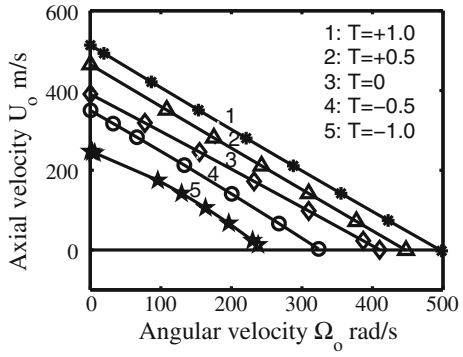

Fig. 12 Correlation curves of the critical axial velocity versus the critical angular velocity with different axial compressive load factors for a simply supported shell, $N = 1$

4 Conclusions

Based on the shell model, dynamics and stability of the inner FGM cylindrical shell conveying a swirling flow in the annular space between the two shells taking into account axial loads are investigated theoretically by the zero-level method in the form of the traveling wave solution. The proposed method is simple and effective by comparing it with the Fourier transform technique. But the purely imaginary roots cannot be obtained by using the method in the calculations.

The results obtained show that the rotation of fluid lowers the critical axial flow speed. And the variation relation of the critical angular velocity versus the critical axial velocity is given. When the axial load is compressive, the overall velocity of losing stability reduces markedly with the increase in the value of the axial load. When the axial load is tensile, the overall velocity of losing stability increases markedly with the increase in the value of the axial load. It is clear that the combined action of the two velocity components and the axial compressive loads makes stable zones become smaller.

The results obtained also show that with the increase of power-law index N the critical flow velocities decrease accordingly.

Also, the critical compressive factors are obtained.

Acknowledgments The authors wish to thank Prof. Shen H.-S. of Shanghai Jiao Tong University for considerable support. The work is supported by grants from National Basic Research Program of China. The authors are grateful for the financial support.

References

1. Tijsseling, A.S., et al.: Fluid-structure interaction in liquid-filled pipe systems: a review. J. Fluids Struct. **10**, 109–146 (1996)
2. Weaver, S.S., et al.: Flow-inducted vibrations in power and process plant components-progress and prospects. J. Press. Vessel. **122**, 339–348 (2000)
3. Païdoussis, M.P., Chan, S.P., Misra, A.K.: Dynamics and stability of coaxial cylindrical shells containing flowing fluid. J. Sound. Vib. **97**, 201–235 (1984)
4. Païdoussis, M.P., Misra, A.K., Chan, S.P.: Dynamics and stability of coaxial cylindrical shells conveying viscous fluid. J. Appl. Mech. **52**, 389–396 (1985)
5. Païdoussis, M.P., Misra, A.K., Nguyen, V.B.: Internal- and annular-flow-induced instabilities of a clamped-clamped or cantilevered cylindrical shell in a coaxial conduit: the effects of system parameters. J. Sound. Vib. **159**, 193–205 (1992)
6. Chebair, E.I.: A., Misra, A.K., Païdoussis, M.P.: Theoretical study of the the effect of unsteady viscous forces on inner- and annular-flow-induced instabilities of cylindrical shells. J Sound. Vib. **138**, 457–478 (1990)
7. Experimental study of annular-flow-induced instabilities of cylindrical shells: EI Chebair, A., Païdoussis, M.P., Misra, A.K. J. Fluids Struct. **3**, 349–364 (1989)
8. Amabili, M., Pellicano, F., Païdoussis, M.P.: Nonlinear dynamics and stability of circular cylindrical shells containing flowing fluid. Part 1. Stability. J Sound. Vib. **225**, 655–699 (1999)
9. Karagiozis, K.N., Païdoussis, M.P., Amabili, M., Misra, A.K.: Nonlinear stability of cylindrical shells subjected to axial flow: theory and experiments. J. Sound. Vib. **309**, 637–676 (2007)
10. Ghayesh, M.H., Païdoussis, M.P., Amabili, M.: Nonlinear dynamics of cantilevered extensible pipes conveying fluid. J. Sound. Vib. **332**, 6405–6418 (2013)
11. Horáĉek, J., Zolotarev, I.: Influence of fixing the edges of a cylindrical shell with conveying fluid on its dynamic characteristics. Int. Appl. Mech. **20**, 756–765 (1984)
12. Horáĉek, J.: Approximate theory of annular flow-induced instability of cylindrical shells. J. Fluids Struct. **7**, 123–135 (1993)

13. Srinivasan, A.V.: Flutter analysis of rotating cylindrical shells immersed in helical circular flowfield of air. AIAA J. **9**, 394–400 (1971)
14. Dowell, E.H., Srinivasan, A.V., Mclean, J.D., Ambrose, J.: Aeroelastic stability of cylindrical shells subjected to a rotating flow. AIAA J. **12**, 1644–1651 (1974)
15. Bochkarev, S.A., Matveenko, V.P.: The dynamic behaviour of elastic coaxial cylindrical shells conveying fluid. J. Appl. Math. Mech. **74**, 467–474 (2010)
16. Bochkarev, S.A., Matveenko, V.P.: Stability analysis of loaded coaxial cylindrical shells with internal fluid flow. Mech. Solids. **45**, 789–802 (2010)
17. Bochkarev, S.A., Lekomtsev, S.V., Matveenko, V.P.: Parametric investigation of the stability of coaxial cylindrical shells containing flowing fluid. Eur. J. Mech. A Solids. **47**, 174–181 (2014)
18. Bochkarev, S.A., Matveenko, V.P.: Stability of a cylindrical shell subjected to an annular flow of rotating fluid. J. Sound Vib. **332**, 4210–4222 (2013)
19. Bochkarev, S.A., Matveenko, V.P.: Stability analysis of cylindrical shells containing a fluid with axial and circumferential components. J. Appl. Mech. Tech. Phys. **53**, 768–776 (2012)
20. Bochkarev, S.A., Matveenko, V.P.: Natural vibrations and stability of a stationary or rotating circular cylindrical shell containing a rotating fluid. Comput. Struct. **89**, 571–580 (2011)
21. Bochkarev, S.A., Matveenko, V.P.: Numerical analysis of stability of a stationary or rotating circular cylindrical shell containing axially flowing and rotating fluid. Int. J. Mech. Sci. **68**, 258–269 (2013)
22. Bochkarev, S.A., Matveenko, V.P.: Specific features of dynamic behavior of stationary and rotating single/coaxial cylindrical shells interacting with the axial and rotational fluid flows. J. Vib. Acoust. **137**, 21001 (2015)
23. Bochkarev, S.A., Matveenko, V.P.: Stability of rotating coaxial cylindrical shells interacting with the flowing and rotating fluid. Int. J. Struct. Stab. Dyn. **15**, 1450071 (2015)
24. Chen, T.L.C., Bert, C.W.: Dynamic stability of isotropic or composite-material cylindrical shell carrying a rotation flow by using travelling wave forms. J. Appl. Mech. **44**, 112–116 (1977)
25. Dao, H.B., Dao, V.D., Vu, H.N., Nguyen, T.P.: Nonlinear static and dynamic buckling analysis of imperfect eccentrically stiffened functionally graded circular cylindrical thin shells under axial compression. Int. J. Mech. Sci. **74**, 190–200 (2013)
26. Chen, W.Q., Bian, Z.G., Ding, H.J.: Three-dimensional vibration analysis of fluid-filled orthotropic FGM cylindrical shells. Int. J. Mech. Sci. **46**, 159–171 (2004)
27. Iqbal, Z., Naeem, M.N., Sultana, N., Arshad, S.H., Shah, A.G.: Vibration characteristics of FGM circular cylindrical shells filled with fluid using wave propagation approach. Appl. Math. Mech. **30**, 1393–1404 (2009)
28. Shah, A.G., Mahmood, T., Naeem, M.N., Arshad, S.H.: Vibrational study of fluid-filled functionally graded cylindrical shells resting on elastic foundations. ISRN Mech. Eng. **2011**, 1–13 (2011)
29. Silva, F.M.A., Montes, R.O.P., Goncalves, P.B., Del Prado, Z.J.G.N.: Nonlinear vibrations of fluid-filled functionally graded cylindrical shell considering a time-dependent lateral load and static preload. J. Mech. Eng. Sci. **230**, 102–119 (2016)
30. Sheng, G.G., Wang, X.: Thermomechanical vibration analysis of functionally graded cylindrical shells with flowing fluid. Eur. J. Mech. A-Solids. **27**, 1075–1087 (2008)
31. Sheng, G.G., Wang, X.: Dynamic characteristics of fluid-conveying functionally graded cylindrical shells under mechanical and thermal loads. Compos. Struct. **93**, 162–170 (2010)
32. Shen, H.J., Païdoussis, M.P., Wen, J.H., et al.: The beam-mode stability of periodic functionally-graded-material shells conveying fluid. J. Sound. Vib. **333**, 2735–2749 (2014)
33. Shen, H.J., Wen, J.H., Yu, D.L., et al.: Stability of fluid-conveying periodic shells on an elastic foundation with external loads. J. Fluids Struct. **46**, 134–148 (2014)
34. Amabili, M.: Nonlinear Vibration and Stability of Shells and Plates. Cambridge University Press, Cambridge (2008)
35. Shun, S.P., Cao, D.Q., Chu, S.M.: Free vibration analysis of thin rotating cylindrical shells using wave propagating approach. Arch. Appl. Mech. **83**, 521–531 (2013)
36. Timoshenko, S.P., Gere, J.M.: Theory of Elastic Stability. McGraw-Hill, New York (1961)